Translational Oncology 58 (2025) 102432

Contents lists available at ScienceDirect

Translational Oncology

journal homepage: www.elsevier.com/locate/tranon

Mitochondrial ribosomal protein L3 (MRPL3): An early diagnostic biomarker and potential molecular target in pancreatic cancer

Mudassier Ahmad [a,b], Sahir Sultan Alvi [a,b], Anupam Dhasmana [a,b], Jasmine Benavidez [a,b], Murali M Yallapu [a,b], Dae Joon Kim [a,b], Subhash C Chauhan [a,b], Bilal Bin Hafeez [a,b,*]

[a] Division of Cancer Immunology, Department of Medicine and Oncology, School of Medicine, University of Texas Rio Grande Valley, McAllen, TX 78504, USA
[b] South Texas Center of Excellence for Cancer Research, School of Medicine, University of Texas Rio Grande Valley, McAllen, TX 78504, USA

ARTICLE INFO

Keywords:
Pancreatic cancer (PanCa)
Mitochondrial ribosomal proteins (MRPs)
Mitochondrial ribosomal protein L3 (MRPL3)
Biomarker
NADH-Ubiquinone Oxidoreductase Core Subunit 1 (NDUFS1)

ABSTRACT

Pancreatic cancer (PanCa) is projected to become the second major cause of cancer-related mortality by 2030. The current diagnostic and treatment strategies offer only marginal benefits in overall survival. This highlights the need to discover new biomarkers and targets for the treatment of PanCa. Dysregulated mitochondrial ribosome biogenesis occurs in PanCa and can be utilized as a potential biomarker and molecular target for its management. In this study, we established MRPL3 (Mitochondrial Ribosomal Protein L3) as a potential biomarker and its role in expression of ETC (Electron Transport Chain) components. We employed an integrated approach combining *the in silico* and experimental validation. Our findings demonstrate that the expression of MRPL3 is upregulated during PanCa in ductal adenocarcinoma and other single cell populations of pancreas. Amongst various grades, the highest expression of MRPL3 was observed in grade 1 human PanCa tumors. MRPL3 is involved in the growth of PanCa cells and the targeted knock-down of MRPL3 leads to decrease in the expression of ETC components. Moreover, *in silico* analysis identified that MRPL3 undergoes alternative splicing that gives rise to six coding and four non-coding variants. The MRPL3–001 isoform arising from ENSG00000114686.8 variant was found to be the most abundant in PanCa. Pathway enrichment analysis showed that MRPL3 is positively associated with cell growth and proliferation while negatively associated with cell lineage commitment and differentiation. These results represent MRPL3 as a promising early biomarker and molecular target for PanCa which warrant further investigation for its clinical applications.

Introduction

Pancreatic cancer (PanCa) remains a significant health burden and third leading cause of cancer-related mortality, with a five-year survival rate of only 11 % [1]. According to American Cancer Society for the year 2025, an estimated 67,440 new cases (34,950 men and 32,490 women) will be diagnosed and 51, 980 people will die of PanCa in the United States [2]. The majority of PanCa cases are classified as adenocarcinomas, primarily pancreatic ductal adenocarcinomas [3]. PanCa is a highly aggressive malignancy characterized by poor prognosis and mortality rate that closely mirrors its incidence rate [4]. Surgical resection remains a primary curative intervention strategy for PanCa; however, >80 % of patients are diagnosed at an advanced stage precluding eligibility for surgical intervention. Notably, early-stage detection could significantly improve survival rates, with estimates suggesting an increase in survival probability of up to 80 % [5,6]. Despite this, no FDA-approved tumor-specific biomarker for PanCa is currently available. Presently, the diagnostic approaches for PanCa rely on multidetector computed tomography (CT) imaging and the serum levels of carbohydrate antigen 19–9 (CA19–9) [7]. However, these

Abbreviations: PanCa, pancreatic cancer; PAAD, pancreatic adenocarcinoma; mtrRNA, Mitochondrial rRNA; MRPs, mitochondrial ribosomal proteins; MRPL3, mitochondrial ribosomal protein L3; NDUFS1, NADH-Ubiquinone Oxidoreductase Core Subunit 1; HR, hazard ratio; TCA, tricarboxylic acid; ETC, electron transport chain; OXPHOS, oxidative phosphorylation; GTEx, Genotype Tissue Expression; KM, Kaplan Meier; TPM, transcripts per million; UMAP, Uniform Manifold Approximation and Projection; GSEA, Gene Set Enrichment Analysis; KEGG, Kyoto Encyclopedia of Genes and Genomes; ATCC, American Type Cell Culture; TMA, tissue micro array; IHC, immunohistochemistry; MCS, mean composite score; IP, immunoprecipitation.

* Corresponding author at: Division of Cancer Immunology, Department of Medicine and Oncology-ISU, South Texas Center of Excellence for Cancer Research, School of Medicine, University of Texas Rio Grande Valley, McAllen, TX 78504, USA.
E-mail address: bilal.hafeez@utrgv.edu (B.B. Hafeez).

https://doi.org/10.1016/j.tranon.2025.102432
Received 14 April 2025; Received in revised form 19 May 2025; Accepted 24 May 2025

methods present inherent limitations. CA19–9, while commonly used, exhibits broad cross-reactivity with multiple malignancies and non-malignant conditions, such as chronic pancreatitis and liver cirrhosis [8]. The available therapeutic regimens, including chemotherapy and targeted therapies are not very effective and are often associated with substantial toxicity in the patients [9]. Consequently, the identification of reliable and specific molecular markers for early detection and prognosis, along with development of new molecular targets remains an urgent clinical need.

Mitochondria are semi-autonomous organelles in the cell that have a separate genome [10]. The mitochondrial DNA encodes the components of electron transfer chain (ETC) or oxidative phosphorylation (OXPHOS). The components of OXPHOS are upregulated in pancreatic and other cancers to increase the survival and proliferation of cancer cells [11]. A dedicated set of ribosomes called mitochondrial ribosomes (mitoribosomes) synthesize the 13 essential proteins of mitochondrial ETC encoded by mitochondrial genome [12]. Mitochondrial ribosomal proteins (MRPs) are structural and functional components of mitoribosomes [13–16]. The MRPs are encoded by the nuclear genome and transported into mitochondria for mitochondrial ribosome biogenesis. The biological role of different MRPs is poorly understood. Emerging evidence suggests that MRPs play a vital role in cancer cell survival and metabolic adaptation [17–19]. Mutations in MRPs have implication in the pathogenesis of several human disorders including neurological disorders, lactic acidosis, and cardiomyopathies [16]. Most of the MRP mutations result in protein instability and defective OXPHOS often leading to early life fatalities. Additionally, mutations in MRPs are also associated with congenital syndromes such as such as blepharophimosis, ptosis, and epicanthus inversus syndrome (BPES), hypogonadism, sensorineural hearing loss, and primary adrenal failure [20]. Particularly, the mutation in MRPL22 in BPES leads to additional deformities such as microcephaly and soft plate cleft. MRPs have been increasingly recognized as contributing factors in the origin, oncogenesis, and cancer progression [21–23]. These molecular alterations suggest that MRPs may serve as potential biomarkers and therapeutic targets for the treatment of cancer. Functional studies in murine models revealed that the knockout of *MRPL3* gene is embryonically lethal, while spontaneous mutations of MRPL3 in decrepit mice lead to neurodegenerative phenotypes. Furthermore, a genome-wide CRISPR/Cas9 screen that MRPs are essential for the viability and growth of cancer cells [24]. Overall, these studies provide a strong clue of MRPs involvement in carcinogenesis and other diseases.

The current study was designed to investigate the role of MRPL3 as an early biomarker and a possible molecular target in PanCa. Our results demonstrate that MRPL3 is overexpressed during the early stages of pancreatic carcinogenesis and its expression correlates with the NADH: Ubiquinone Oxidoreductase Core Subunit 1 (NDUFS1) in human pancreatic tumors. NDUFS1 is the part of complex I of ETC that transfers electrons from NADH to OXPHOS [25]. Targeted knockdown of MRPL3 inhibits the growth of PanCa with concomitant decrease of both NDUFS1 and ATPase8. *In silico* analysis revealed the presence of various coding and non-coding isoforms of MRPL3 in PanCa, which are associated with the pathways involved in growth and differentiation.

Materials and methods

Chemicals and reagents

All cell culture media and analytical grade reagents used in this study were obtained from commercial sources. Dulbecco's Modified Eagle Medium (DMEM)-high glucose (Cat. No 11,965,092), Roswell Park Memorial Institute (RPMI) 1640 (Cat. No 11,875,093), DMEM/F-12 Medium (Cat. No 11,320,033), McCoy's 5A (Modified) medium (Cat. No 16,600,082), fetal bovine serum (FBS) (Cat. No 10,437–028), Trypsin EDTA (0.25 %) with phenol red (Cat. No 25,200,056), phosphate buffer saline (PBS)-pH 7.4 (Cat. No 10,010,023), and antibiotic-antimycotic (100X) (Cat. No 15,240,062) were procured from Gibco™ by Life Technologies, Carlsbad, CA, USA. Eagle's Minimum Essential Medium (EMEM; Cat. No 30–2003) was procured from American Type Culture Collection (ATCC, Manassas, Virginia, USA). For immunohistochemical (IHC) analysis, the peroxidazed-1 (Cat. No PX968M), Diva Decloaker RTU (Cat. No DV2004G1), background sniper (Cat. No BS966M), DaVinci Green antibody diluent (Cat. No PD900M), MACH 4 Universal HRP-Polymer (Cat. No M4U534G), 3,3′-Diaminobenzidine (DAB) chromogen kit (Cat. No DB801), and CAT Hematoxylin (Cat. No CATHE-M) were obtained from BioCare Medical LLC, Pacheco, CA, USA.

Antibodies

The following primary antibodies were used in this study: anti-MRPL3 (Cat. No *Sc*-514,217, Santa Cruz Biotechnology Inc, CA, USA), anti-NDUFS1 (Cat. No 12,444-I-AP, ProteinTech Group Inc, IL, USA), anti-ATPase8 (Cat. No 26,723-I-AP, ProteinTech Group Inc, IL, USA). Normal mouse IgG (Cat. No *Sc*-2025, Santa Cruz Biotechnology Inc, CA, USA) was used as an isotype control IgG. The secondary antibodies utilised in this study were: anti-Rabbit IgG HRP conjugate (Cat. No W401B) and anti-mouse IgG HRP conjugate (Cat. No W402B) from Promega, Madison, WI, USA.

Normal organ-specific MRPL3 gene expression coverage, overall survival, and reference-test gene correlation analysis

The organ and tissue-specific expression profile of MRPL3 under normal physiological conditions was analyzed by utilizing Genotype Tissue Expression (GTEx) database [26]. Kaplan Meier (KM) survival analysis was conducted using the KM Plotter tool to evaluate the prognostic significance of MRP3 expression in pancreatic adenocarcinoma (PAAD) [27]. Furthermore, pairwise gene correlation analysis between two genes MRPL3 and NDUFS1 (test genes) was performed in PAAD tissues using gene transcript per million (TPM) values, as retrieved from the Gene Expression Profiling Interactive Analysis (GEPIA) database [28].

Spot prediction of MRPL3 in single cell type cluster of pancreatic cells

The cellular location of MRPL3 within pancreas cell cluster was evaluated using single-cell RNA sequencing (scRNA-seq) data, employing Uniform Manifold Approximation and Projection (UMAP) analysis [29]. This approach facilitated the spatial prediction of MRPL3 expression across distinct cell clusters of pancreatic cells. The expression distribution was assessed within a range of 0–210 nTPM values, with cellular abundance represented in terms of read count and total cell count.

Analysis of MRPL3 coding structures and gene isoforms

The structural diversity and isoform-specific expression pattern of MRPL3 in PAAD were assessed by using the isoform analysis sub module of GEPIA2 [30]. The genomic transcript data of GEPIA2 was obtained from The Cancer Genome Atlas (TCGA) database. GEPIA2 contains comprehensive genomic information, encompassing a total of 60,498 genes and 198,619 isoforms, categorized into distinct classes such as protein-coding, retained introns, and processed transcript, etc. [31].

Analysis of MRPL3 associate co-expressed genes

To investigate MRPL3-associated co-expressed genes and their functional enrichment, the LinkFinder and LinkInterpreter sub-modules of LinkedOmics were employed [28,32]. LinkFinder enabled gene association analysis, while LinkInterpreter facilitated enrichment analysis. RNA-seq data ($n = 178$) from the University of North Carolina (UNC) were analyzed using Spearman's correlation coefficient and visualized

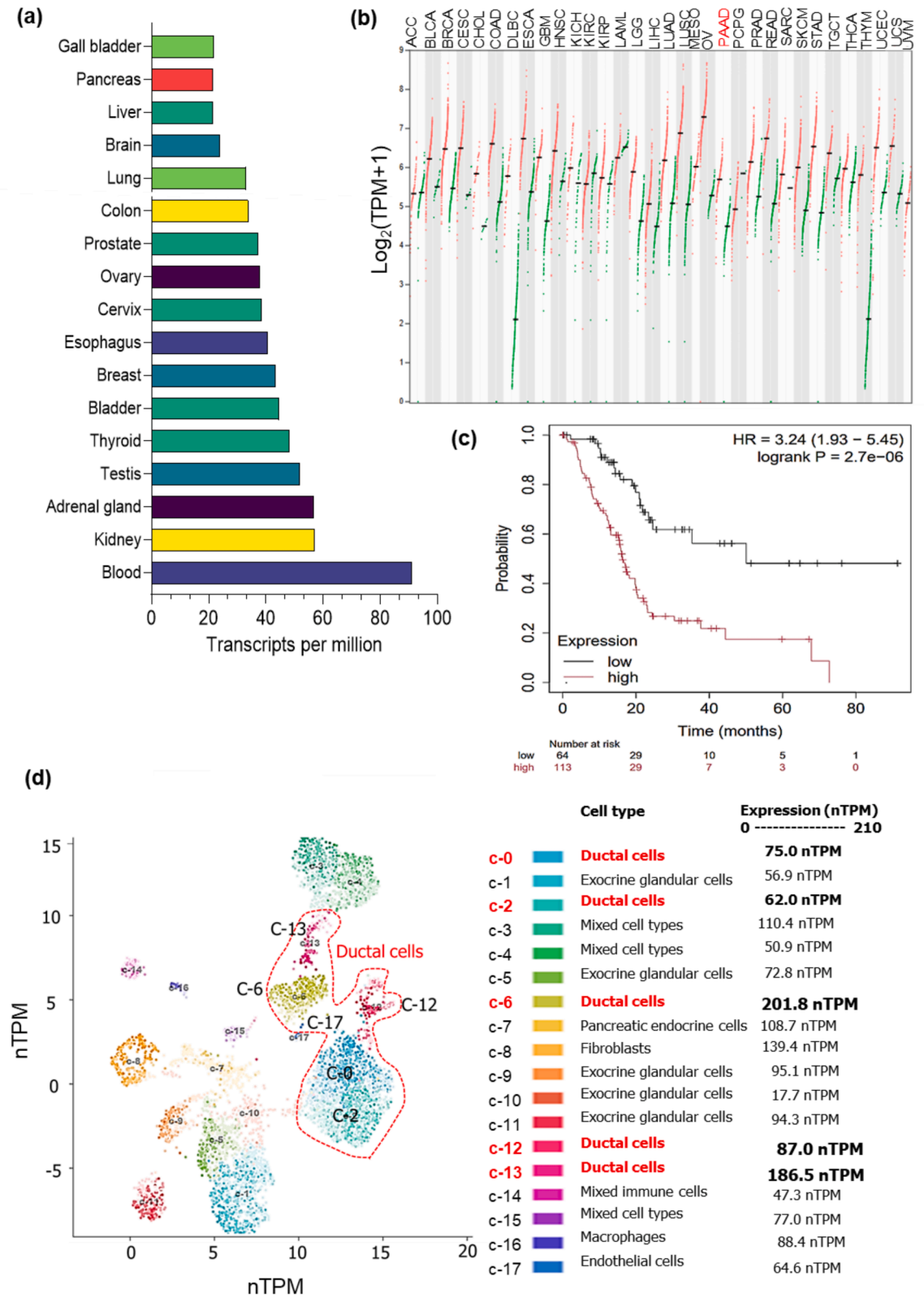

Fig. 1. Expression profiling of MRPL3 in normal and cancerous tissues. (a) The bar graph shows the organ-specific expression of MRPL3 in humans. The data was obtained from Gene Expression Profiling Interactive Analysis (GEPIA) database (http://gepia.cancer-pku.cn/) and plotted with GrapPad Prism version 10.0.0. software. **(b)** The expression of MRPL3 was studied in different cancers which shows that the expression of MRPL3 is increased in many cancers (red dots) as compared to normal condition (green dots). The data was obtained from GEPIA database. **(c)** The Kaplan Meier plot shows that the survival rate is very poor in PanCa patients with MRPL3 overexpression. The Hazard ratio (HR) is >2 (indicative of very poor survival rate) and Logrank P value is 0.0012. **(d)** MRPL3 positioning in pancreas: RNA expression of MRPL3 in various pancreatic tissues. The single cell type clusters identified in this tissue were visualized by a UMAP plot.

via volcano plots. Genes exhibiting significant positive or negative correlation with MRPL3 were identified based on a statistical threshold of $p < 0.01$ [33]. Gene enrichment analysis was conducted using Gene Set Enrichment Analysis (GSEA) database within the Kyoto Encyclopedia of Genes, and Genomes (KEGG) Pathways plugin. The enrichment analysis parameters included a minimum of 25 IDs per category, a maximum of 2000 IDs per category, selection of the top 25 significant categories, and 10,000 permutations.

Cell culture

The pancreatic cancer cell lines Capan-2, AsPC-1, MIA PaCa-2, HPAF-II, BxPC-3, PANC-1, and non-cancerous HPNE cells were obtained from ATCC. The cell lines were cultured in their suggested growth media supplemented with 10 % FBS and 1 % antibiotic. The cells were maintained at 37 °C in a humidified atmosphere containing 5 % CO_2 [34].

Immunohistochemistry

The paraffin embedded human pancreatic tissue microarray (TMA) slide was processed for analysis. The slides were rehydrated by immersing into an ethyl alcohol gradient and then subjected to 0.3 % H_2O_2 (peroxidazed-1) and subsequently 1 % Triton X-100. The heat-induced antigen retrieval was done using the universal decloaking solution at 120 °C for 20 min followed by blocking with the Blocking Sniper for 30 min at RT and then primary antibodies (MRPL3 diluted in DaVinci Green Ab diluent; dilution 1:100) were applied to the slides, incubated at RT for 1 h and followed by overnight incubation at 4 °C. MACH 4 Universal HRP probe and polymer were applied to the slides for appropriate duration and washed with TBS. After washing the unbound secondary antibodies, a few drops of DAB substrate were applied to the slides to detect the immunoreactive complexes and then the slides were counterstained by CAT hematoxylin, dehydrated in alcohol gradient, mounted after cleaning with xylenes and the images were captured by using PANNORAMIC Digital Slide Scanner (PANNORAMIC MIDI II) by 3DHISTECH Ltd.

Western blotting

Western blotting was done as previously reported [35]. Cells were seeded in 100 mm culture dishes and allowed to reach 70–80 % confluency. After completion of the incubation cells were harvested, and protein estimation was done by Pierce BCA Protein Assay. The samples were denatured in the heat block pre-set at 95 °C for 5 min. 20–40 μg protein of each sample was loaded in precast gels from Bio-Rad depending upon the size of protein. The membranes were blocked for 1.5 to 2 h in 5 % blocking buffer (non-fat dry milk or BSA in TBST). The membranes were incubated overnight with primary antibodies at 4 °C with gentle rocking (~20 rpm). After this, incubation with secondary antibody was done for 1 hour at room temperature (R.T.). Protein bands on the membranes were detected using. Immobilon western chemiluminescent HRP substrate (Millipore, Cat. No WBKLS0500) was used for imaging the membranes and imaged using ChemiDoc imager (BioRad, CA, USA).

Generation of MRPL3 knockdown stable cells

MIA PaCa-2 cells seeded in 6 -well plates were transfected either with scrambled (Scr) or MRPL3 shRNA packed into lentiviruses (Cat. No sc-77,897-V, Santa Cruz Biotechnology Inc, CA, USA) at a multiplicity of infection equal to 1. After 24 h, the reduced serum medium was removed, and cells were allowed to grow overnight in supplemented DMEM media. The selection was done using puromycin at 1.0 μg/mL for 7 days with the media change every alternate day. The generation of stable MRPL3 KD clones was verified by western blotting.

Confocal microscopy

HPNE, MIA PaCa-2 and HPAF-II cells were seeded in 24-well plates on sterile Corning® BioCoat® Poly-l-Lysine glass coverslips as described recently [1]. After attachment, cells were incubated with Invitrogen's MitoTracker™ dye RedFM (Cat No M22425), ThermoFisher Scientific, MA, USA) for 45 min. The cells were then fixed with 4 % paraformaldehyde followed by permeabilization with 0.25 % Triton X-100 for 10 min. The cells were washed thrice and blocked with 1 % BSA for 30 min at R.T. After blocking, MRPL3 (1:200) and NDUFS1 (1:200) antibodies were added and left overnight at 4 °C. The cells were washed thrice with PBS for 5 min each and incubated with FITC -labelled anti-mouse secondary Antibody from Invitrogen, Waltham, MA Cat. No 62–6511; dilution-1:200) or Alexa Fluor® 647 labelled anti-rabbit secondary antibody from Jackson Immuno-Research Laboratories, Inc., Pennsylvania, USA (Cat. No 711–606–152; dilution-1:100) for 1 hour at R.T. The cells were washed thrice, mounted on glass slides using VECTASHIELD Vibrance® Antifade Mounting Medium with DAPI by Vector Laboratories, Inc., CA, USA (Cat. No H-1800–2). The slides were left for 15 min at R.T. for hardening and then stored at 4 °C in dark boxes. The images were acquired on Leica STELLARIS STED & STELLARIS 8 STED Microscope, Leica Microsystems (Wetzlar, Germany).

Immunoprecipitation (IP)

Two million cells were seeded in 100 mm culture dishes. The cells were processed in the same way as in western blotting. After protein estimation, equal volume (1 mL) of samples in RIPA buffer containing 200 μg of protein were precleared with 20 μL of protein A-Agarose beads (Santa Cruz, Cat. No sc-2001) at 4 °C for 1 h. 10 μg of MRPL3 antibody and 20 μL of magnetic protein A/G-Agarose beads (Santa Cruz, Cat. No sc-48,385) was added to IP samples. Normal mouse IgG (Santa Cruz, Cat. No sc-2025) was used as an isotype control. The samples were incubated overnight at 4 °C with rotation. The samples were denatured for 5 min at 95 °C. 10 μL of samples were loaded on the precast gels and processed as per the western blotting protocol mentioned above. The membranes were probed with NDUFS1 antibody and incubated overnight at 4 °C, followed by probing with secondary antibody for 1 hour at R.T. Immobilon western chemiluminescent HRP substrate (Millipore, Cat. No WBKLS0500) was used to image the membrane on ChemiDoc imager (BioRad, CA, USA).

Statistical analysis

The statistical significance was calculated by a two-tailed unpaired *t*-test using GraphPad Prism version 10.0.0. The p values are expressed as $*p \leq 0.05$, $**p \leq 0.01$, $***p \leq 0.001$, and $****p \leq 0.0001$ [36].

Results

MRPL3 overexpression is associated with high risk of mortality in PanCa patients

The oncogenic role of MRPL3 was not studied in cancer. In this study, we investigated the potential of MRPL3 as an early biomarker and molecular target in PanCa. We analyzed the expression of MRPL3 in various human organs, different pancreatic cells, and normal and pancreatic tumor tissues using *in silico* approaches. MRPL3 expression was within the range of 21.55 to 91 TPM (transcripts per million) in various normal human tissues (Fig. 1**a**). Among all the investigated organs, gall bladder, pancreas, liver, and brain showed comparatively low expression of MRPL3, whereas prostate, ovaries, and cervix displayed intermediate expression. In contrast, the blood cells exhibited the highest MRPL3 expression. Further, *in silico* analysis revealed significant ($p < 0.01$) increase of MRPL3 expression in pancreatic tumor tissues as compared to normal pancreatic tissues (Fig. 1**b**). A similar trend was observed across

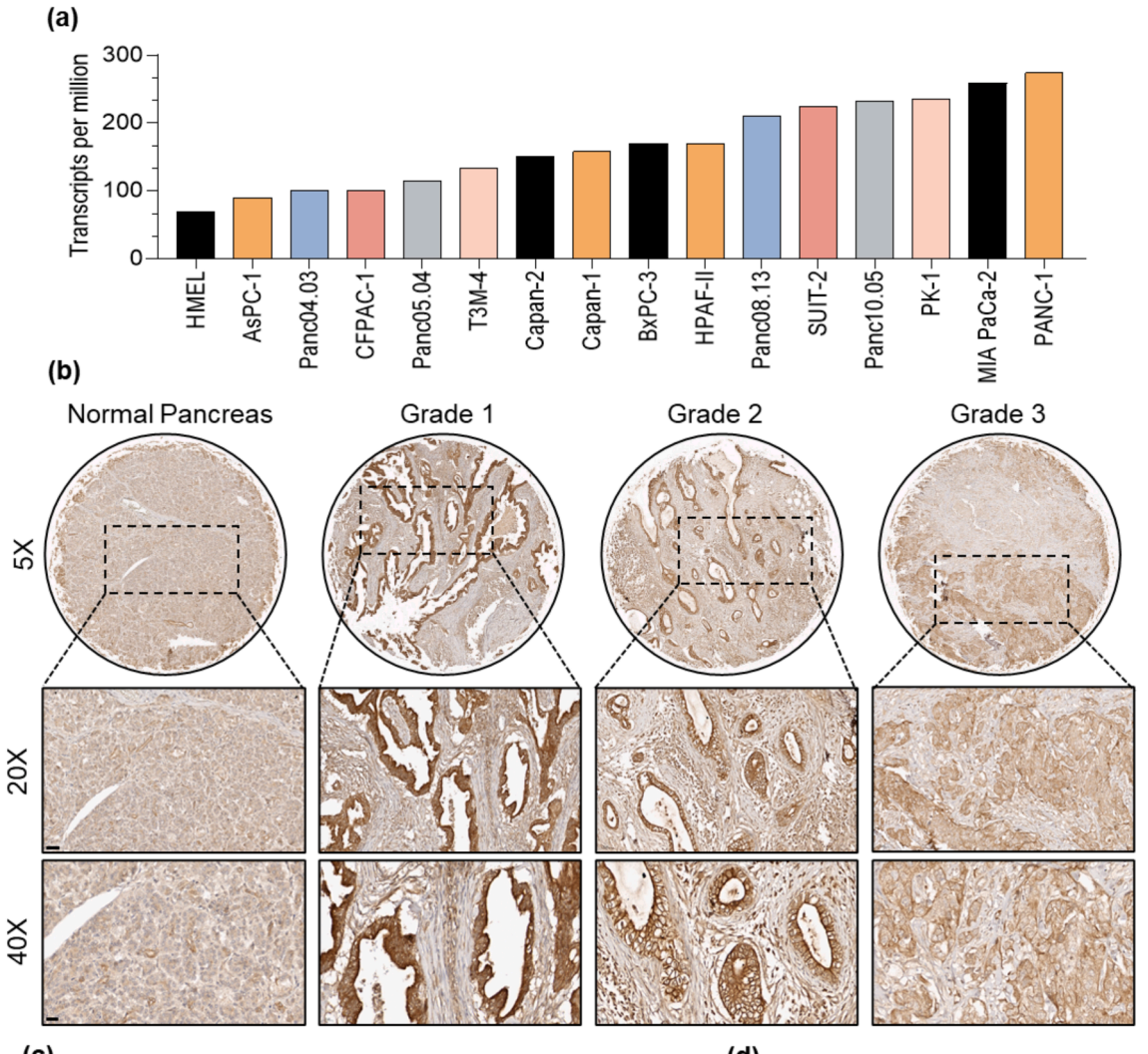

(c)

Groups	No. of specimens	Weak	Moderate	Strong	Very strong
Normal	9	9 (100%)	0 (0%)	0 (0%)	0 (0%)
NAT	10	10 (100%)	0 (0%)	0 (0%)	0 (0%)
Low grade (grade 1, grade 1-2)	11	0 (0%)	0 (0 %)	3 (27.3 %)	4 (36.4%)
Medium grade (grade 2, grade 2-3)	23	0 (0%)	10 (43.5%)	7 (30.4%)	6 (26.1%)
High grade (grade 3)	12	0 (0%)	5 (41.6 %)	5 (41.6%)	2 (16.7 %)

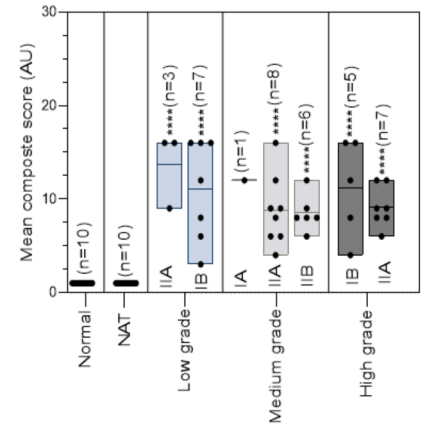

Fig. 2. Expression profiling of MRPL3 in normal and cancerous tissues. (a) PanCa cell lines show differential expressions of MRPL3. RNA seq data was obtained from the European Bioinformatics Institute database (https://www.ebi.ac.uk/gxa/home). Primary human mammary epithelial line (HMEC) was used as a control. **(b).** The representative images from IHC analysis of PanCa TMA Shows that the MRPL3 expression increases in Grade 1, 2, and 3 of PanCa as compared to normal pancreatic tissues. The scale bars in IHC micrographs correspond to 50 μm and 20 μm at 20X and 40X magnifications, respectively. **(c)** The table shows the level of MRPL3 expression in normal, NAT, and PanCa tissues from different grades. The level of MRPL3 expression was calculated from the IHC staining shown in Fig. 2(b). **(d)** Mean composite score (MCS) of normal and cancerous pancreatic tissues belonging to different stages of grade1, grade 2 and grade 3 of PanCa. MCS was calculated to analyze the expression of MRPL3 in different areas of pancreatic normal and cancer samples The p values were calculated by comparing MCS of PanCa tissues with normal samples. The number of samples (n) used for the analysis is indicated in the figure. The p values are expressed as ***$p \leq 0.001$ ****$p \leq 0.0001$.

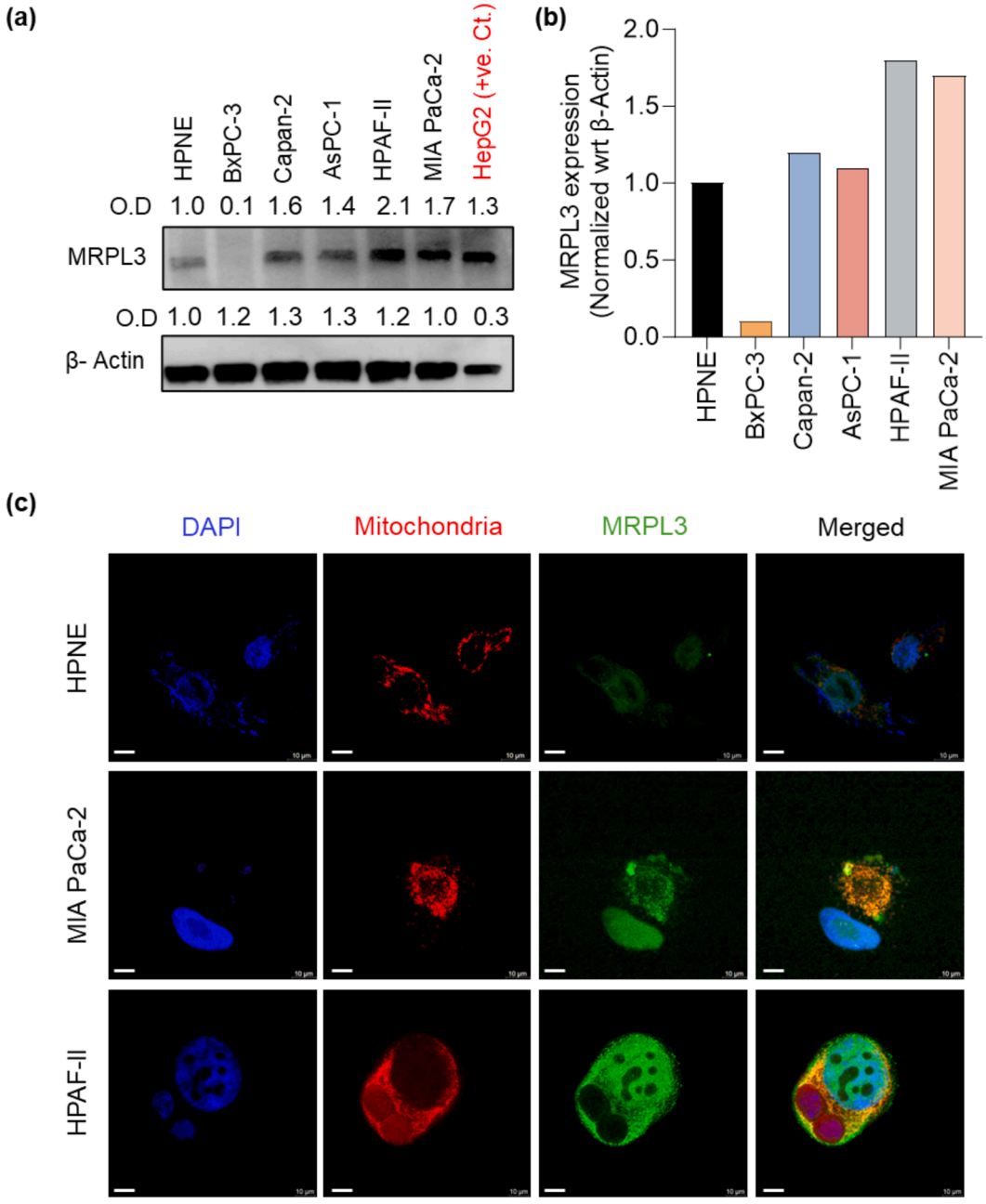

Fig. 3. MRPL3 is overexpressed in PanCa cells. (a) Expression of MRPL3 in pancreatic immortalized-normal (HPNE) and cancer cell lines was analyzed by western botting. The expression of MRPL3 in each cell line was analyzed by Image J and the values were represented as O.D. above the blots. **(b)** Densitometry analysis of MRPL3 expression**. (c)** Localization of MRPL3 (green) was studied by immunofluorescence confocal microscopy in HPNE, MIA- PaCa-2, and HPAF-II cells. Nucleus were labelled with DAPI (Blue) and mitochondria with Mito tracker RedFM (Red) dyes. Magnification scale bar represents 10 μm.

multiple cancer types compared to respective normal counterparts (Fig. 1**b and Supplementary Table 1**). Next, we examined the correlation of MRPL3 with overall survival of PanCa patients. The results indicated that the elevated expression of MRPL3 is linked with poor overall survival in PanCa patients compared to patients with lower expressing MRPL3. This relationship was quantified using the hazard ratio (HR), a clinical metric that gene expression level with patient outcomes (Fig. 1c) [37]. Specifically, H.$R > 1$ indicates low survival rate due to treatment or increased gene expression, H.$R = 1$ denotes no effect of treatment or increased gene expression and H.$R < 1$ signifies high survival due to treatment or increased gene expression. These results strongly suggest the association of increased expression of MRPL3 with higher mortality in PanCa patients. Given the heterogeneity of pancreatic tissue, which comprises both endocrine and exocrine components with diverse cell populations. We further evaluated the expression of MRPL3 at the single cell level using UMAP plot (Fig. 1**d**). This UMAP plot analysis identified that PDAC cells have the highest expression of MRPL3 among all pancreatic cells (exocrine glandular cells, fibroblasts, immune cells, macrophages, and endothelial cells). Overall, these computational results provide a strong clue of MRPL3 association with overall less survival rate in PanCa patients.

Validation of MRPL3 in silico results by wet lab findings

Using RNA-seq data from the European Bioinformatics Institute database (https://www.ebi.ac.uk/gxa/home), we observed that PanCa cell lines express greater MRPL3 as compared to normal cells (HMEL) (Fig. 2**a**). To corroborate the above *in silico* results, we investigated the

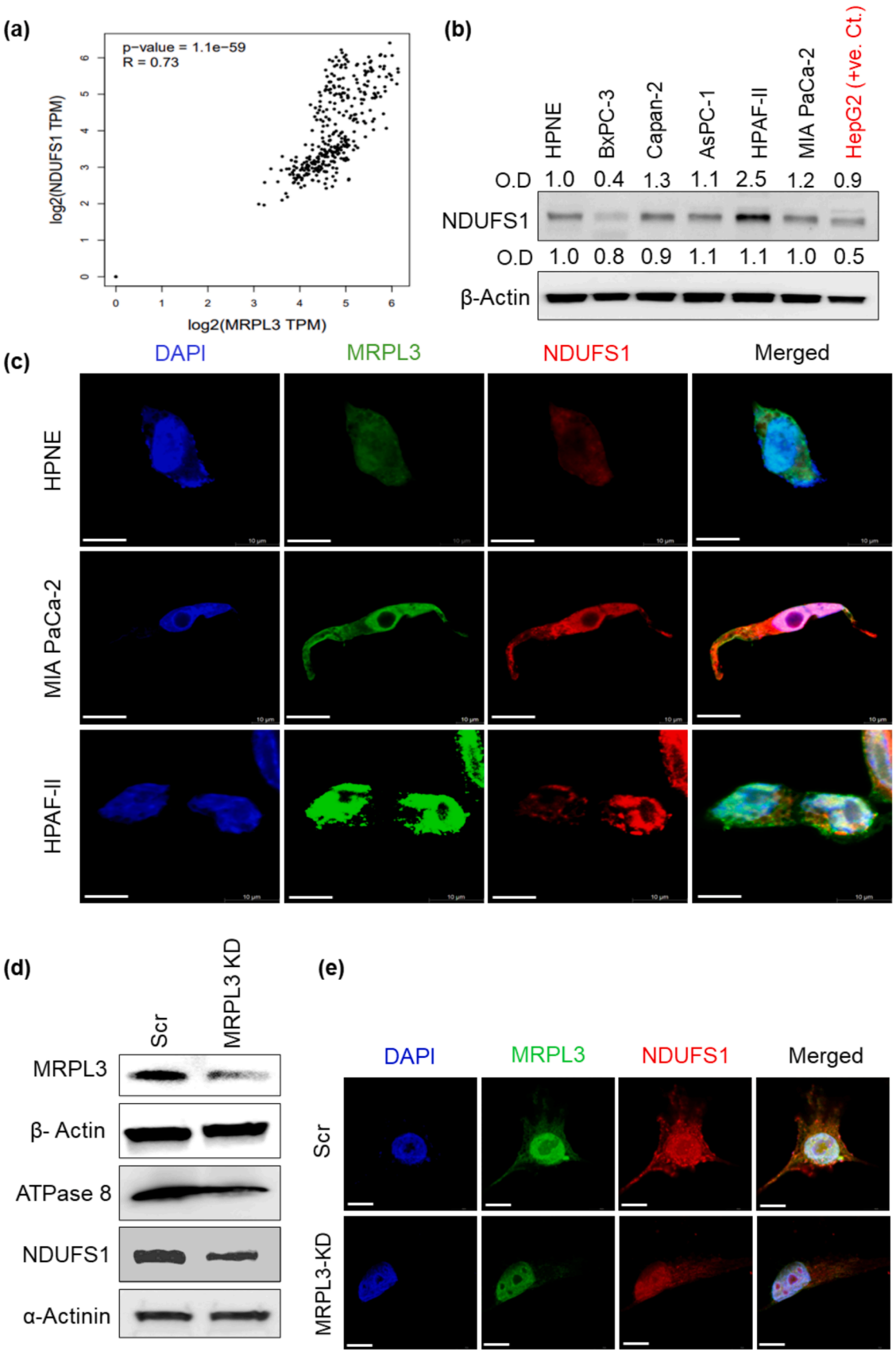

(caption on next page)

Fig. 4. MRPL3 KD decreases the expression of ETC components. (a) The correlation analysis of MRPL3 and NDUFS1 was done by using GEPIA database (http://gepia.cancer-pku.cn/). MRPL3 and NDUFS1 are positively correlated with spearman coefficient (R) value equal to 0.73. **(b)** Differential gene expression of NDUFS1 in HPNE and PanCa lines was studied by western botting. The expression of NDUFS1 in each cell line was analyzed by Image J and the values were represented as O.D. above the blots. **(c)** Co-localization of NDUFS1 (red) and MRPL3 (green) was studied by double-immunofluorescence confocal microscopy in HPNE, MIA- PaCa-2 and HPAF-II cells. Magnification scale bar represents 10 μm. **(d)** Stable MRPL3 KD clones were generated by infecting the MIA PaCa-2 cells shRNA coated with lentivirus. After selection with puromycin (1 μg/mL), the expression of MRPL3 in the stable clones was analyzed by western blotting. The effect of MRPL3 KD on expression of ATPase 8 and NDUFS1 (ETC components) in MIA PaCa-2-MRPL3 KD stable clones was detected by western blotting. **(e)** Effect of MRPL3 KD on the localization of NDUFS1 and MRPL3 in MIA PaCa-2-MRPL3 KD stable clones was detected by confocal microscopy. Magnification scale bar represents 10 μm.

expression level of MRPL3 in pancreatic tissues by IHC. Our results exhibited high expression of MRPL3 protein in all grades/stages of PanCa as compared to the normal pancreatic tissues (Fig. 2**b**). The intensity of IHC staining was graded as 1, 2, 3, and 4 denoting weak, moderate, strong, and very strong MRPL3 expression, respectively (Fig. 2**c**). All the grades 1 and 1–2 pancreatic tumor tissues showed the highest MRPL3 protein level, while pancreatic tumor grades 2, 2–3, and 3 showed moderate, strong and very strong protein levels of MRPL3. However, all the normal and normal adjacent tissues (NAT) of pancreas showed weak expression of MRPL3 (Fig. 2**c**). To consider the differences in MRPL3 expression across the different regions of the samples, we calculated mean composite score (MCS) of samples belonging to the various grades of PanCa (Fig. 2**d and Supplementary Table 2**). Coverage denotes the expression of MRPL3 in the different areas of a tissue section. The coverage was categorized as 1, 2, 3, and 4 which denotes weak, moderate, strong and very strong coverage of tissue sections by MRPL3 signal during IHC staining. Like our intensity data, normal pancreatic and NAT samples showed the least MCS score equal to 1. On the other hand, grade 2, grade 2–3, and grade 3 tissue samples showed several fold increases in MCS of MRPL3 compared to normal and NAT tissues. Overall, our results clearly indicate that MRPL3 is highly overexpressed in the early stage of PanCa.

MRPL3 is overexpressed in PanCa cells

MRPL3 is a mitochondrial protein expressed in the nuclei of the cells. To confirm the *in silico* analysis data, we determined the expression of MRPL3 in transformed human pancreatic normal epithelial (HPNE) and various PanCa cells (BxPC3, Capan-2, AsPC1, HPAF-II, and MIA PaCa-2) by Western blot analysis. Our results demonstrated that MRPL3 is differentially upregulated in PanCa cells as compared to HPNE cells. The highest expression of MRPL-3 was observed in MIA PaCa-2 and HPAF-II cells, while Capan-2 and AsPC-1 cells show moderate expression of MRPL3 (Fig. 3**a and** 3**b, and supplementary Fig. 1**). However, BxPC-3 cells did not show any detectable protein level of MRPL3. We further investigated the localization of MRPL3 in normal and pancreatic cells using confocal microscopy. We observed that MRPL3 was predominantly localized in mitochondria in both normal (HPNE) and PanCa cells (i.e., MIA PaCa-2 and HPAF-II) (Fig. 3**c**). To investigate the functional impact of MRPL3 in PanCa cells, we generated MRPL3-knockdown (MRPL3 KD) MIA PaCa-2 stable cell line and characterized by western blot analysis (Fig. 3**c**). These results indicate that MRPL3 is differentially expressed in human PanCa cells.

MRPL3 regulates the expression of ETC proteins

MRPL3 is one of the critical components of mitoribosomes which are involved in the synthesis of ETC proteins. We hypothesized that MRPL3 might have a role in the expression of ETC components. To investigate this hypothesis, we first performed *in silico* analysis to investigate the correlation between MRPL-3 and complex I ETC protein NDUFS1. Using correlation database GEPIA, we found that the expression of MRPL3 is positively correlated with the expression of NDUFS1 ($R = 0.73$) (Fig. 4**a**). Next, we determined the expression of NDUFS1 in HPNE and various PanCa cells (BxPC3, Capan-2, AsPC1, HPAF-II, and MIA PaCa-2 by Western blot analysis. Our results revealed that NDUFS1 is overexpressed in all the tested PanCa cells (Capan-2, AsPC1, HPAF-II, and MIA PaCa-2) compared to HPNE cells (Fig. 4**b; supplementary Fig. 2 and 3**). The double immunofluorescence analysis of MRPL3 and NDUFS1 in HPNE, MIA PaCa-2, and HPAF-II cells demonstrated co-localization of MRPL3 and NDUFS1 in PanCa cells compared to HPNE (Fig. 4**c**). To further evaluate if MRPL3 and NDUFS1 proteins physically interact in PanCa cells, we performed immunoprecipitation/WB analysis. Our results revealed no direct physical interaction of MRPL3 and NDUFS1 proteins in HPAF-II cells (**Supplementary Fig. 4**). NDUFS1 and ATPase 8 are critical components of mitochondrial functionality, where NDUFS1 is involved in mitochondrial respiration, while ATPase 8 is critical for ATP production [25,38] . Therefore, we determined if MRPL3 is involved in regulating NDUFS1 and ATPase 8. Our results revealed that targeted knockdown of MRPL3- inhibited the expression of both NDUFS1 and ATPase 8 in MIA PaCa-2 cells (Fig. 4**d and supplementary Fig. 5**). Confocal microscopy results also revealed a decreased expression of NDUFS1 in MRPL3 KD cells compared to control (Fig. 4**e**). Overall, these results suggest that MRPL3 expression correlates with NDUFS1 and targeted knockdown of MRPL3 inhibits ETC components in PanCa cells.

MRPL3 gene expresses several isoforms and regulates the signaling pathways involved in PanCa development and growth

Genetic information is diversified by the production of protein isoforms by alternative gene splicing [39]. Previous studies have shown that various isoforms of MRPs are involved in important cellular functions such as protein stability [40]. Therefore, we were interested to know if MRPL3 isoforms are present in PanCa. Our *in silico* analysis data showed the presence of six coding and four non-coding variants of MRPL3 (Fig. 5**a**). The six coding variants were found to translate into isoforms. Out of the six MRPL3 isoforms, ENST000026995.7, was identified as the most abundant MRPL3 splice variant in PanCa (Fig. 5**b**). To understand the role of MRPL3 isoforms in PanCa, we investigated the association of MRPL3 with co-expressed genes using the LinkFinder and LinkInterpreter. RNA-seq data from the TCGA_PAAD cohort and the UNC Institute dataset were processed using the HiSeq RNA platform and the Firehose_RSEM_log2 pipeline. The study identified a total of 19,695 enriched genes, of which 11,857 exhibited significant negative correlations with MRPL3 (green dots), while 7838 genes showed significant positive correlations (red dots) (Fig. 5**c**). Functional enrichment analysis using GSEA and KEGG pathway categories within LinkInterpreter revealed that MRPL3 co-expressed genes were significantly associated with multiple biological processes (Fig. 5**d**).

The pathways positively correlated with MRPL3 included ribosome, RNA transport, aminoacyl-tRNA biosynthesis, cell cycle, DNA replication, ribosome biogenesis in eukaryotes, proteasome, protein processing in the endoplasmic reticulum, nucleotide excision repair, and homologous recombination. Conversely, pathways negatively correlated with MRPL3 included chemokine signaling, osteoclast differentiation, neuroactive ligand-receptor interaction, staphylococcus aureus infection, cell adhesion molecules (CAMs), intestinal immune network for IgA production, NF-kappa B signaling, hematopoietic cell lineage, Th1 and Th2 cell differentiation, and cytokine-cytokine receptor interaction. Overall, these results demonstrate that MRPL3 splice variants may have a role in the development and growth of PanCa.

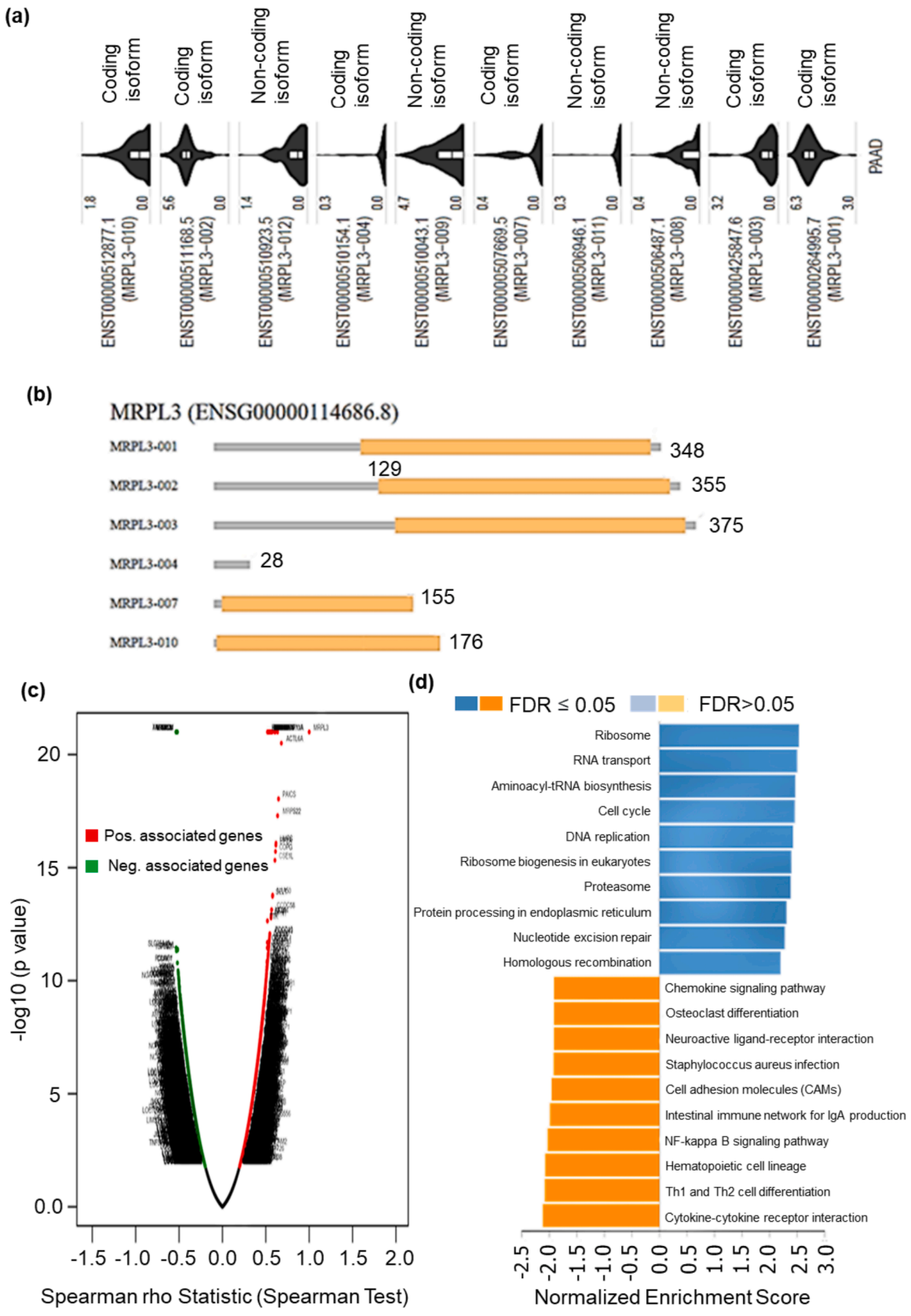

Fig. 5. MRPL3 isoforms regulate key signaling pathways. (a-b) MRPL3 mRNA undergoes alternative splicing that generates ten splice variants. Six coding isoforms arise from splice variants. The splice variants that give rise to coding or non-coding isoforms of MRPL3 have been labelled in Fig. 5a. The structures of coding-isoforms have been shown in Fig. 5b **(c)** Volcano plot shows the genes significantly correlated with MRPL3. The correlation was done by Spearman test. Green and red dots represented the negative and positive correlations with MRPL3, respectively. **(d)** Pathway enrichment analysis of MRPL3 and associated genes was done by using LinkInterpreter. Blue and orange bar graphs represent pathway enrichment of genes positively and negatively associated with MRPL3.

Discussion

Despite the progress made, the incidence and mortality associated with PanCa continue to show an upward trend unlike most other cancers. This health concern could be addressed by the discovery of new biomarkers and targets for PanCa. The use of mitochondrial ribosome biogenesis components as early clinical biomarkers and molecular targets for PanCa has not been reported. Accumulating evidence suggests the role of MRPs in tumorigenesis and metabolic reprogramming [41–44]. Several MRPs exhibit altered expressions in various cancers, influencing mitochondrial function, apoptosis, and cellular stress responses. Given their differential expression in normal versus tumor tissues [20]. However, little is known about the role of MRPs in PanCa. A recent *in silico* study has shown that overexpression of MRPL3 is associated with poor prognosis of PanCa [45]. Our results demonstrate a significant increase in MRPL3 expression in different cancers including PanCa. *In silico* single cell RNA seq and IHC analysis revealed that expression of MRPL3 is higher in pancreatic ductal cells than other single cell populations of pancreas. The expression of MRPL3 was higher in grade I PanCa tissues indicating use as a potential early biomarker for PanCa. The increased expression of MRPL3 was found to be associated with decreased chances of survival as indicated by H.R of 3.24. These results confirm that an increase in MRPL3 expression can also be used as a potential biomarker for poor prognosis in PanCa. The correlation between KRAS and mitochondrial metabolism in growth of cancer cells and tumorigenesis has been previously reported [46]. The expression of MRPL3 was found to be low in BxPC-3 PanCa cells which harbor wild type *KRAS* than PanCa cells (Capan-2, AsPC-1, HPAF-II and MIA PaCa-2) express mutated *KRAS*. Further studies are warranted to establish the role of *KRAS* in overexpression of MRPL3 in PanCa.

MRPL3 is expressed in the nuclei of pancreatic cells and translocated to mitochondria for synthesis of mitoribosomes. CRISPR/Cas9 deletion screening has shown that mitochondrial proteins are important for the growth of tumor cells [24]. Available literature shows that antibiotics such as tetracyclines inhibit mitochondrial protein synthesis [47,48]. A pharmacological screening has shown that pyrvinium pamoate, an anthelmintic drug, inhibits mitochondrial respiration in acute myeloid leukemia cells by targeting OXPHOS proteins [49]. The essentiality of MRPs may be attributed to the involvement of mitoribosomes in translation of ETC components [50]. NDUFS1 is a part of complex I of ETC that transfers electrons from NADH to ETC [51]. MRPL3 KD in PanCa was found to decrease the expression of both NDUFS1 and ATPase 8 proteins. These results indicates that MRPL3 is involved in translational efficiency of mitoribosomes which promotes the cell death via decreasing expression of ETC components. However, further detailed mechanistic investigations are warranted to fully understand the correlation between MRPL3 and ETC components.

The splice variants of ribosomal genes have been linked to the survival of cancer cells and are emerging molecular targets for cancer therapeutics [52]. The uL10β isoform of uL10 ribosomal protein have been found to be associated with ER stress [39]. Two MRPL12 isoforms have been shown to be involved in transcriptional regulation of mitochondrial genes and mitochondrial ribosome biogenesis [40]. Our study indicates the presence of both non-coding and coding variants of MRPL3 in PanCa. However, more in depth study is required to understand and molecular mechanisms and functional impact of these coding and non-coding isoforms of MRPL3 in PanCa. MRPLs play an important role in diverse cellular processes such as OXPHOS and apoptosis. Our results demonstrate correlation of MRPL3 with signaling pathways associated with cell cycle, DNA replication, aminoacyl-tRNA biosynthesis, and ribosome biogenesis. While the genes negatively correlated with MRPL3 promote the pathways associated to cell lineage and differentiation such as hematopoietic cell lineage, osteoclast differentiation, and Th1 and Th2 differentiation.

Conclusion

MRPL3 is overexpressed in early-stage pancreatic tumor tissues and its expression correlates with the expression of NDUFS1. Targeted knockdown of MRPL3 inhibits expression of both NDUFS1 and ATPase8. Overall, this study suggests that MRPL3 could be the potential early-stage biomarker and molecular target in PanCa. Targeting mitoribosome biogenesis through MRPL3 could be a novel strategy for the prevention and treatment of PanCa.

Compliance with ethics requirement

Not applicable.

Data availability

All the data generated has been included either in this article or provided as supplementary information. Further information and requests for resources and reagents should be directed to the lead contact, Dr. Bilal B. Hafeez (bilal.hafeez@utrgv.edu).

CRediT authorship contribution statement

Mudassier Ahmad: Writing – review & editing, Writing – original draft, Visualization, Validation, Software, Methodology, Investigation, Formal analysis, Data curation, Conceptualization. **Sahir Sultan Alvi:** Writing – review & editing, Software, Methodology, Investigation, Formal analysis, Data curation. **Anupam Dhasmana:** Writing – review & editing, Methodology, Formal analysis, Data curation. **Jasmine Benavidez:** Writing – review & editing, Methodology, Data curation. **Murali M Yallapu:** Writing – review & editing, Visualization. **Dae Joon Kim:** Data curation, Formal analysis, Resources, Writing – review & editing. **Subhash C Chauhan:** Writing – review & editing, Visualization. **Bilal Bin Hafeez:** Writing – review & editing, Writing – original draft, Visualization, Validation, Supervision, Resources, Project administration, Methodology, Investigation, Funding acquisition, Formal analysis, Data curation, Conceptualization.

Declaration of competing interest

The authors declare that they have no conflict of interest.

Acknowledgements

This study was supported by NIH/NIGMS (Grant No SC1GM140982–01) and CPRIT (Grant No RP230454) grants awarded to Dr. Bilal Bin Hafeez. We also acknowledge the Integrated Cancer Research Core (ICRC), South Texas Center of Excellence for Cancer Research, SOM, UTRGV, supported by UT System and CPRIT (Grant No RP210180 and #RP230419).

Supplementary materials

Supplementary material associated with this article can be found, in the online version, at doi:10.1016/j.tranon.2025.102432.

References

[1] A.A. Bangash, et al., Honey targets ribosome biogenesis components to suppress the growth of human pancreatic cancer cells, Cancers (Basel) 16 (19) (2024) 3431.
[2] Cancer Facts & Figures, American Cancer Society, Atlanta, 2025.
[3] S. Wang, et al., The molecular biology of pancreatic adenocarcinoma: translational challenges and clinical perspectives, Signal Transduct. Targeted Therapy 6 (1) (2021) 249.
[4] W. Sang, et al., Receptor-interacting protein kinase 2 is an immunotherapy target in pancreatic cancer, Cancer Discov. 14 (2) (2024) 326–347.

[5] A.L. Blackford, et al., Recent trends in the incidence and survival of stage 1A pancreatic cancer: a surveillance, epidemiology, and end results analysis, J. Natl. Cancer Inst. 112 (11) (2020) 1162–1169.
[6] E.M. Stoffel, R.E. Brand, M. Goggins, Pancreatic cancer: changing epidemiology and new approaches to risk assessment, early detection, and prevention, Gastroenterology, 164 (5) (2023) 752–765.
[7] J.J. Cheng, et al., Differential expression of CD175 and CA19-9 in pancreatic adenocarcinoma, Sci. Rep. 15 (1) (2025) 4177.
[8] S. Kim, et al., Carbohydrate antigen 19-9 elevation without evidence of malignant or pancreatobiliary diseases, Sci. Rep. 10 (1) (2020) 8820.
[9] T. Conroy, et al., FOLFIRINOX versus gemcitabine for metastatic pancreatic cancer, N. Engl. J. Med. 364 (19) (2011) 1817–1825.
[10] M. Chong, et al., GWAS and ExWAS of blood mitochondrial DNA copy number identifies 71 loci and highlights a potential causal role in dementia, eLife 11 (2022).
[11] T.M. Ashton, et al., Oxidative phosphorylation as an emerging target in cancer therapy, Clin. Cancer Res. 24 (11) (2018) 2482–2490.
[12] D.L. Rudler, et al., Fidelity of translation initiation is required for coordinated respiratory complex assembly, Sci. Adv. 5 (12) (2019) eaay2118.
[13] Y.S. Bykov, et al., Widespread use of unconventional targeting signals in mitochondrial ribosome proteins, EMBO J. 41 (1) (2022) e109519.
[14] A. Ferrari, S. Del'Olio, A. Barrientos, The diseased mitoribosome, FEBS Lett. 595 (8) (2021) 1025–1061.
[15] H.J. Kim, P. Maiti, A. Barrientos, Mitochondrial ribosomes in cancer, Semin. Cancer Biol. 47 (2017) 67–81.
[16] B.J. Greber, N. Ban, Structure and function of the mitochondrial ribosome, Annu. Rev. Biochem. 85 (2016) 103–132.
[17] K. Prokopidis, et al., Aberrant mitochondrial homeostasis at the crossroad of musculoskeletal ageing and non-small cell lung cancer, PLoS One 17 (9) (2022) e0273766.
[18] R.P. Oviya, et al., Mitochondrial ribosomal small subunit (MRPS) MRPS23 protein-protein interaction reveals phosphorylation by CDK11-p58 affecting cell proliferation and knockdown of MRPS23 sensitizes breast cancer cells to CDK1 inhibitors, Mol. Biol. Rep. 49 (10) (2022) 9521–9534.
[19] F. Sotgia, M.P. Lisanti, Mitochondrial biomarkers predict tumor progression and poor overall survival in gastric cancers: companion diagnostics for personalized medicine, Oncotarget 8 (40) (2017) 67117–67128.
[20] G. Huang, H. Li, H. Zhang, Abnormal expression of mitochondrial ribosomal proteins and their encoding genes with cell apoptosis and diseases, Int. J. Mol. Sci. 21 (22) (2020).
[21] M. Ghoussaini, et al., Evidence that the 5p12 variant rs10941679 confers susceptibility to estrogen-receptor-positive breast cancer through FGF10 and MRPS30 regulation, Am. J. Hum. Genet. 99 (4) (2016) 903–911.
[22] D. Criscuolo, et al., Targeting mitochondrial protein expression as a future approach for cancer therapy, Front. Oncol. 11 (2021) 797265.
[23] R.H. Malty, et al., Mitochondrial targets for pharmacological intervention in human disease, J. Proteome Res. 14 (1) (2015) 5–21.
[24] L.W. Thomas, et al., Genome-wide CRISPR/Cas9 deletion screen defines mitochondrial gene essentiality and identifies routes for tumour cell viability in hypoxia, Commun. Biol. 4 (1) (2021) 615.
[25] R. Elkholi, et al., MDM2 integrates cellular respiration and apoptotic signaling through NDUFS1 and the mitochondrial network, Mol. Cell 74 (3) (2019) 452–465, e7.
[26] The GTEx Consortium atlas of genetic regulatory effects across human tissues, Science 369 (6509) (2020) 1318–1330.
[27] B. Győrffy, Integrated analysis of public datasets for the discovery and validation of survival-associated genes in solid tumors, Innovation (Camb) 5 (3) (2024) 100625.
[28] A. Dhasmana, et al., CEACAM7 expression contributes to early events of pancreatic cancer, J. Adv. Res. 55 (2024) 61–72.
[29] M. Uhlén, et al., Proteomics. Tissue-based map of the human proteome, Science 347 (6220) (2015) 1260419.
[30] Z. Tang, et al., GEPIA: a web server for cancer and normal gene expression profiling and interactive analyses, Nucleic. Acids. Res. 45 (W1) (2017) W98–w102.
[31] A. Dhasmana, et al., Integrative big transcriptomics data analysis implicates crucial role of MUC13 in pancreatic cancer, Comput. Struct. Biotechnol. J. 21 (2023) 2845–2857.
[32] S.V. Vasaikar, et al., LinkedOmics: analyzing multi-omics data within and across 32 cancer types, Nucleic. Acids. Res. 46 (D1) (2018) D956–d963.
[33] B. Wu, et al., Gene regulation network of prognostic biomarker YAP1 in human cancers: an integrated bioinformatics study, Pathol. Oncol. Res. 27 (2021) 1609768.
[34] R. Nabi, et al., Modulatory role of HMG-CoA reductase inhibitors and ezetimibe on LDL-AGEs-induced ROS generation and RAGE-associated signalling in HEK-293 Cells, Life Sci. 235 (2019) 116823.
[35] M. Chaib, et al., Reprogramming of pancreatic adenocarcinoma immunosurveillance by a microbial probiotic siderophore, Commun. Biol. 5 (1) (2022) 1181.
[36] M. Waiz, S.S. Alvi, M.S. Khan, Association of circulatory PCSK-9 with biomarkers of redox imbalance and inflammatory cascades in the prognosis of diabetes and associated complications: a pilot study in the Indian population, Free Radic. Res. 57 (4) (2023) 294–307.
[37] H. Barraclough, L. Simms, R. Govindan, Biostatistics primer: what a clinician ought to know: hazard ratios, J. Thorac. Oncol. 6 (6) (2011) 978–982.
[38] C. Panja, et al., Analysis of MT-ATP8 gene variants reported in patients by modeling in silico and in yeast model organism, Sci. Rep. 13 (1) (2023) 9972.
[39] K. Filipek, et al., Identification of a novel alternatively spliced isoform of the ribosomal uL10 protein, Biochim Biophys Acta Gene Regul Mech 1866 (1) (2023) 194890.
[40] J. Nouws, et al., Mitochondrial ribosomal protein L12 Is required for POLRMT stability and exists as two forms generated by alternative proteolysis during import, J. Biol. Chem. 291 (2) (2016) 989–997.
[41] F. Morais-Rodrigues, et al., Analysis of the microarray gene expression for breast cancer progression after the application modified logistic regression, Gene 726 (2020) 144168.
[42] Q. Zhang, et al., Differentially expressed mitochondrial genes in breast cancer cells: potential new targets for anti-cancer therapies, Gene 596 (2017) 45–52.
[43] M.C. Caino, D.C. Altieri, Molecular pathways: mitochondrial reprogramming in tumor progression and therapy, Clin. Cancer Res. 22 (3) (2016) 540–545.
[44] M. Peiris-Pagès, et al., Mitochondrial and ribosomal biogenesis are new hallmarks of stemness, oncometabolism and biomass accumulation in cancer: mito-stemness and ribo-stemness features, Aging (Albany NY) 11 (14) (2019) 4801–4835.
[45] K. Chen, et al., Gene signature associated with neuro-endocrine activity predicting prognosis of pancreatic carcinoma, Mol. Genet. Genomic. Med. 7 (7) (2019) e00729.
[46] F. Weinberg, et al., Mitochondrial metabolism and ROS generation are essential for Kras-mediated tumorigenicity, Proc. Natl Acad. Sci. 107 (19) (2010) 8788–8793.
[47] S.N. Dijk, et al., Mitochondria as target to inhibit proliferation and induce apoptosis of cancer cells: the effects of doxycycline and gemcitabine, Sci. Rep. 10 (1) (2020) 4363.
[48] M. Škrtić, et al., Inhibition of mitochondrial translation as a therapeutic strategy for human acute myeloid leukemia, Cancer Cell 20 (5) (2011) 674–688.
[49] J. Decroocq, et al., RAS activation induces synthetic lethality of MEK inhibition with mitochondrial oxidative metabolism in acute myeloid leukemia, Leukemia 36 (5) (2022) 1237–1252.
[50] J.E. Sylvester, et al., Mitochondrial ribosomal proteins: candidate genes for mitochondrial disease, Genet. Med. 6 (2) (2004) 73–80.
[51] R.M. Gill, et al., Protein S-glutathionylation lowers superoxide/hydrogen peroxide release from skeletal muscle mitochondria through modification of complex I and inhibition of pyruvate uptake, PLoS One 13 (2) (2018) e0192801.
[52] Z. Feng, et al., Targeting colorectal cancer with small-molecule inhibitors of ALDH1B1, Nat. Chem. Biol. 18 (10) (2022) 1065–1075.